Published online 9 December 2017

Nucleic Acids Research, 2018, Vol. 46, No. 5 ***e25***
doi: 10.1093/nar/gkx1222

Multimode drug inducible CRISPR/Cas9 devices for transcriptional activation and genome editing

Jia Lu[1,2,†], Chen Zhao[1,†], Yingze Zhao[1,†], Jingfang Zhang[1,†], Yue Zhang[1], Li Chen[1,2], Qiyuan Han[1], Yue Ying[1], Shuai Peng[1,3], Runna Ai[1] and Yu Wang[1,2,*]

[1]State Key Laboratory of Stem Cell and Reproductive Biology, Institute of Zoology, Chinese Academy of Sciences, Beijing 100101, China, [2]University of Chinese Academy of Sciences, Beijing 100049, China and [3]Qufu Normal University, Qufu 273165, China

Received June 09, 2017; Revised October 26, 2017; Editorial Decision November 23, 2017; Accepted November 27, 2017

ABSTRACT

Precise investigation and manipulation of dynamic biological processes often requires molecular modulation in a controlled inducible manner. The clustered, regularly interspaced, short palindromic repeats (CRISPR)/CRISPR associated protein 9 (Cas9) has emerged as a versatile tool for targeted gene editing and transcriptional programming. Here, we designed and vigorously optimized a series of Hybrid drug Inducible CRISPR/Cas9 Technologies (HIT) for transcriptional activation by grafting a mutated human estrogen receptor (ER^{T2}) to multiple CRISPR/Cas9 systems, which renders them 4-hydroxytamoxifen (4-OHT) inducible for the access of genome. Further, extra functionality of simultaneous genome editing was achieved with one device we named HIT2. Optimized terminal devices herein delivered advantageous performances in comparison with several existing designs. They exerted selective, titratable, rapid and reversible response to drug induction. In addition, these designs were successfully adapted to an orthogonal Cas9. HIT systems developed in this study can be applied for controlled modulation of potentially any genomic loci in multiple modes.

INTRODUCTION

Taking advantage of their RNA-guided DNA binding and endonuclease activity, CRISPR/Cas9 systems have been adapted to sequence dependent modulations in the genomic contexts (1–3). Cas9 protein binds and cleaves DNA in a sequence specific manner based on its complementarity with the associated guide RNA (gRNA) and the adjacent presence of a protospacer-adjacent motif (PAM). DNA cleavage mediated by the Cas9–gRNA complex results in targeted gene editing, either through error prone non-homologous end-joining (NHEJ) or precise homology directed repair (HDR) (1–3). Further, utilities of the CRISPR/Cas9 systems have been expanded to other molecular functions, including transcription activation, repression, genomic DNA labeling, and epigenetic programming, by coupling with various effectors (4,5). For these purposes, DNA cleavage is spared by using nuclease-null, or 'dead', Cas9 (dCas9) variants bearing key mutations in nuclease domains, while the DNA binding activity that recruits the effectors to target loci is retained (2). CRISPR-Cas9 dependent gene transcriptional activation system can be achieved by recruiting activation domains (ADs) to the dCas9–gRNA complex. Around 20 ADs and their combinations have been screened for activation potential (6,7). Commonly used ADs include VP64 (an engineered tetramer of the herpes simplex virus transcriptional activator domain VP16), p65 (NF-κB transactivating subunit), Rta (immediate-early nuclear transcription factor of Kaposi's sarcoma-associated herpesvirus), HSF1 (human heat-shock factor 1), and their combinations VPR (VP64, p65 and Rta) and PH (p65 and HSF1) (3,5–16). To date, there are multiple strategies to generate dCas9–gRNA directed transcriptional activation systems, including direct fusion of ADs to dCas9 and recruitment of multiple AD modules to a peptide array fused with dCas9 or aptamers appended to gRNAs (3,5–16).

Precise dissection of dynamic biological processes often requires perturbation of the underlying molecular events in a controlled inducible manner. Greater precision is also beneficial towards the translational ends for development of gene therapies. Nuclear hormone receptors, estrogen receptor (ER) as a representative, have been adapted to drug inducible genome modulation, which utilizes their ligand dependent translocation from the cytoplasm to the nucleus (17). Without its hormone ligand, ER is sequestered by heat shock protein Hsp90 in the cytoplasm. Ligand

*To whom correspondence should be addressed. Tel: +86 10 82619461; Fax: +86 10 82619461; Email: yuwang@post.harvard.edu
†These authors contributed equally to this work as first authors.
Present address: Yingze Zhao, National Institute for Viral Disease Control and Prevention, Chinese Center for Disease Control and Prevention, Beijing 102206, China.

binding disrupts their interaction, thus leading to ER translocation to the nucleus. ER bearing three mutations G400V/M543A/L544A, also known as ER^{T2}, displays selective affinity to the synthetic estrogen antagonist 4-OHT over β-estradiol, the endogenous ER ligand, a property crucial for low background activity (18). As its best known application, ER^{T2} fusion to the Cre recombinase has been widely used in biomedical research for conditional and inducible genome engineering (19,20).

Here we established and comprehensively optimized a series of novel drug inducible transcriptional activation systems, which we named Hybrid Inducible CRISPR/Cas9 Technologies (HIT) based on coupling CRISPR/Cas9 and ER^{T2}. 4-OHT inducible transcriptional activation was first accomplished using various CRISPR/Cas9 systems grafted with ER^{T2} domains. Then simultaneous gene activation and editing was delivered in drug inducible manner using one device termed HIT2. These systems delivered better performances than several designs published previously in head-to-head comparisons (21–24). Consistent with these findings, multiple latest literatures reported Cas9 editing activity under the tight control of the ER domain (25–27). We also demonstrated that drug induction is titratable, selective, rapid, and reversible. Further, architectures developed in this study can be applied directly to orthogonal Cas9 devices. HIT-Cas9 systems developed herein provide powerful tools for controlled modulation of potentially any genomic loci in multiple modes.

MATERIALS AND METHODS

Plasmid construction

Cas9, dCas9 and ER^{T2} were cloned from the pX330-U6-Chimeric_BB-CBh-hSpCas9 plasmid (a gift from Feng Zhang, Addgene plasmid # 42230 (1)), the pMSCV-LTR-dCas9-VP64-BFP plasmid (a gift from Stanley Qi & Jonathan Weissman, Addgene plasmid # 46912 (15)) and the pAd-CreER plasmid (a gift from T.C. He's lab, Chicago University), respectively. Multiple activation domains (ADs), including VP64(V), P65(P), Rta(R) and HSF1(H), were cloned from Addgene plasmids (VP64 was PCR amplified from pLenti-EF1a-SOX2, a gift from Feng Zhang, Addgene plasmid #35388 (28); P65 and Rta were amplified from SP-dCas9-VPR, a gift from George Church, Addgene plasmid # 63798 (7); HSF1 was amplified from lenti MS2-P65-HSF1_Hygro, a gift from Feng Zhang, Addgene plasmid # 61426 (6)). scFv-sfGFP-GB1 and 10xGCN4 were synthesized (Genewiz) according to the sequences reported by Tanenbaum *et al.* (11). MCP plasmids were cloned by replacing scFv with MCP, which was cloned from MCP-P65-HSF1, a gift from Feng Zhang, Addgene plasmid # 61426 (6)). NES were synthesized (Sangon Biotech) according to the sequence reported by Ding *et al.* (29) and inserted into various Cas9 constructs. As for scFv constructs used in simultaneous gene editing and gene activation, we removed sfGFP so that it did not interfere with GFP fluorescence from BFP editing. TRE3G promoter was cloned from the Tet-On 3G inducible expression system from Clontech. Intein-S219-G521R was a gift from David Liu (Addgene plasmid # 64192 (24)). As for intein-S219-G521R-VPR construction, intein-G521R was inserted in dCas9 at S219 and VPR were fused to the C-terminus of dCas9. Split-Cas9, split-dCas9(N) and split-dCas9-VP64(C) were gifts from Feng Zhang (Addgene plasmid # 62889 (23); Addgene plasmid # 62887 (23); Addgene plasmid # 62888 (23)). SaCas9-2NES-2ER^{T2}-GCN4 plasmids were cloned by replacing SpCas9 with SaCas9 (a gift from Feng Zhang, Addgene plasmid # 61591 (30)). NLS-dSaCas9–GCN4 and NLS-dSaCas9-VPH plasmids were cloned by replacing dCas9 with dSaCas9 (a gift from Feng Zhang, Addgene plasmid # 61594 (30)). Key plasmids of HIT systems reported in this study will be available through Addgene.

sgRNA candidates for both gene activation and editing were chosen based on prediction of high efficiency and low off-target effect by the computational analyses using the GPP web portal (http://www.broadinstitute.org/rnai/public/analysis-tools/sgrna-design) (31,32) and the CRISPR DESIGN web portal (http://crispr.mit.edu/) (33). They are cloned into an optimized single chimeric guide RNA scaffold (A-U flip extension) (34) and experimentally examined for their potency using the pSSA assay and endogenous gene activation assays respectively for editing and activation purposes (data not shown). One sgRNA displaying highest activity was chosen for each gene (Supplementary Table S1). sgRNA2.0s for the SAM system were cloned using a backbone plasmid from Feng Zhang (Addgene plasmid # 61424) (6). sgRNAs candidates of SaCas9 for both gene editing and activation were chosen by PAM sequence requirement (NNGRRT) (Supplementary Table S3) (30). They were cloned into an optimized single chimeric guide RNA scaffold (A-U flip) (35) and experimentally examined in the pSSA assay and transcriptional activation assays for activity (data not shown).

The pSSA reporter plasmids used in this study to examine Cas9 DNA cleavage activity were constructed by insertion of sgRNA target sequences in between the homology domains (36).

The TLR plasmid was constructed by replacing Sce target with sgRNA targeting sequence in the plasmid of pCVL Traffic Light Reporter 1.1 (Sce target) Ef1a Puro (a gift from Andrew Scharenberg Addgene plasmids #31482) (37). GFP donor plasmid used in conjunction was a gift from Andrew Scharenberg (Addgene plasmids #31475) (37).

The gLuc luciferase reporter plasmid used in this study to examine gene activation activity was constructed by inserting the gLuc sgRNA target sequence (Supplementary Table S1) upstream of a minimal CMV promoter (pAAV-minCMV-mCherry was a gift from Feng Zhang, Addgene plasmid # 27970 (28)), and replacing mCherry with firefly luciferase or gaussia luciferase. The gaussia luciferase reporter plasmid used in this study to examine gene activation activity via SaCas9 was constructed by replacing gLuc sgRNA target sequence with the target sequence of a telomere sgRNA in the gaussia luciferase reporter (Supplementary Table S3).

The BFP reporter plasmid used in FCR assay to examine gene editing activity was constructed by mutagenesis of the 198th–200th nucleotides TAC in GFP ORF to CAT using a plasmid containing EF1a-GFP cassette (38).

Cell culture

HEK293T cells (ATCC) were maintained in Dulbecco's modified Eagle's Medium supplemented with 10% FBS, 2 mM GlutaMAX (Thermo Fisher), 100 U/ml penicillin and 100 μg/ml streptomycin under 37°C, 5% CO_2. Stable monoclonal cell lines of TLR and FCR reporters were generated following standard protocols of lentivirus packaging and infection. Transfections were done using Biotool DNA transfection Reagent (Biotool) according to the manufacturer's recommended protocol. Within each experiment, the molar amount of each AD and the total weight of transfected DNA were matched for each well. Unless stated otherwise, culture medium was changed 5 h after transfection with 125 nM of 4-OHT or a matched volume of ethanol. Cells were cultured for additional 48 h before examination of genome editing or transcription activation.

Transcription activation assays

For luciferase reporter assay, HEK293T cells were plated into 96-well plates. A total plasmid mass of 183 ng was transfected using 0.45 ul of Biotool DNA transfection Reagent (Biotool) for each well according to the manufacturer's instructions. The molar amount of sgRNA, dCas9, and ADs were matched across all wells. Constitutive expression plasmids of renilla luciferase and firefly luciferase were co-transfected to serve as internal control for firefly luciferase and gaussia luciferase respectively. Culture medium containing 125 nM 4-OHT was changed 5 h after transfection. Forty eight hours after 4-OHT was added, samples were incubated with luciferase substrates (Promega for firefly luciferase; New England Biolabs for gaussia and renilla luciferase) and then analyzed using Victor*X*3 Multilabel Plate Reader (PerkinElmer) according to the manufacturer's recommended protocol.

As for endogenous gene activation, HEK293T cells were plated into 24-well plates. Cells were cultured, transfected using standard protocols. The total amount of transfected DNA and the molar amount of sgRNA, dCas9 and ADs were all matched across all wells. Forty eight hours after 4-OHT was added, cells were harvested from each transfection and subsequently processed for total RNA extraction using the Direct-zol™ RNA MiniPrep Kit (Zymo Research). cDNA was generated using the GoScript cDNA Synthesis Kit (Promega) according to the manufacturer's recommended protocol. mRNA expression levels were quantitated using SYBR Green Gene Expression Assays (Toyobo). The sequences of qPCR primers were listed in Supplementary Table S2. As for the CD43 activation assay, 48 h after 4-OHT was added, live cells were collected and incubated with a CD43 antibody conjugated with APC (Miltenyi Biotec) according to the manufacturer's recommended protocol. Then cells were analyzed by the CytoFLEX (Beckman Coulter).

Subcellular localization analyses

HEK293T cells were cultured on 24-well plates. 500 ng of scFv-2E-V or scFv-2E-PH was transfected into each well. To examine C2N2E-GCN4 localization, 400 ng of scFv-GFP were transfected alone or co-transfected with 400 ng of C2N2E-GCN4 into each well. Cells were then transferred to 96-well plates for image collection after 48 h induction of 4-OHT. Images were collected and quantitatively analyzed using Operetta High Content Screening system (PerkinElmer) after cells being fixed by 4% (w/v) paraformaldehyde and stained with Hochest 33342 (Thermo Fisher).

Gene editing assays

As for the pSSA reporter assay, HEK293T cells were cultured, transfected using standard protocols. Forty eight hours after transfection, 50 ul medium was collected and then gaussia luciferase substrate (New England Biolabs) was added. A constitutive expression plasmid of firefly luciferase was co-transfected to serve as a normalization control. Luciferase activity was measured by chemical luminescence using VICTOR *X*3 Multi-label Plate Reader (PerkinElmer) according to the manufacturer's recommended protocol.

As for the TLR assays, 250 ng of various Cas9 constructs and 150 ng of sgRNA with or without 400 ng of GFP donor template (Addgene plasmids #31475 (37)) were co-transfected into each well of TLR reporter cells pre-seeded on 24-well plates. HDR assessment was done with flow cytometry analysis using CytoFLEX cell analyzer (Beckman Coulter). 50 000 cells at the minimum from each well were analyzed. The HDR rates were determined by the percentiles of GFP positive cells. Cells were transferred to 96-well plates for NHEJ measurements. Images were collected using Operetta High Content Screening system (PerkinElmer) after cells being fixed by 4% (w/v) paraformaldehyde and stained with Hochest 33342 (Thermo Fisher). The mCherry fluorescence was assessed by Harmony 3.5 (Perkin-Elmer).

As for the CD201 genomic knockout assay, HEK293T cells were cultured, transfected using standard protocols. Twenty four hours after transfection, transfected cells were enriched by antibiotic selection using 125 ug/ml Zeocin and 100 ug/ml G418. Twenty four hours after selection, 4-OHT was added. Cells were cultured for several days till reaching sufficient amount for live staining with a CD201 antibody conjugated with PE-Vio770 (Miltenyi Biotec) and flow cytometry analysis using the CytoFLEX (Beckman Coulter).

As for the FCR assay, the stable cell line was cultured on 24-well plates. 300 ng of various Cas9 constructs and 300 ng of BFP sgRNA with 10 pmol of ssDNA donor template were co-transfected into each well. The sequence of donor template was 5′-GCCACCTACGGCAAGCTGACCCTGAAGTTCA TCTGCACCACCGGCAAGCTGCCCGTGCCCTGG CCCACCCTCGTGACCACCCTGACGTACGGCGT GCAGTGCTTCAGCCGCTACCCCGACCACATGA-3′ (38) (synthesized by Sangon Biotech). HDR assessment was performed with flow cytometry analysis using CytoFLEX cell analyzer (Beckman Coulter). At least 30,000 cells from each well were analyzed. The HDR rates were determined by the percentiles of GFP positive cells.

Assay of simultaneous BFP editing and CD43 activation

BFP stable cell line was used for simultaneous BFP editing and CD43 activation. Cells were cultured in 24-well

plates and transfected using standard protocols. The total amount of transfected DNA and the molar amount of CD43 and BFP sgRNAs, Cas9 fusions, and activators were all matched across all wells. 10 pmol ssDNA donor was co-transfected to each well. Forty eight hours after 4-OHT introduction, live cells were collected and stained with a CD43 antibody conjugated with APC (Miltenyi Biotec) according to the manufacturer's recommended protocol. Then cells were examined using the CytoFLEX (Beckman Coulter).The efficiencies of BFP editing and CD43 activation were determined by the percentages of GFP and CD43 positive cells respectively.

RESULTS

Drug inducible transcriptional activation

In order to efficiently evaluate various designs for gene activation, we constructed a luciferase reporter under control of a sgRNA target sequence (gLuc sgRNA) (Supplementary Figure S1A) (39). Transcription machineries are exclusively accessible in the nucleus, thus drug inducible performance of our HIT-dCas9 activation systems can be readily assessed upon co-transfection with this reporter construct. Using it as a surrogate, we first optimized designs within each system. Next the designs delivering the most tight and efficient drug inducible performance from each system were compared side by side for the activation of the luciferase reporter and a panel of endogenous genes.

The most straightforward design for CRISPR/Cas9 based transcription activation utilized direct AD fusion to dCas9 (3,7–9,14–16). dCas9-VP64 represents the first generation of this kind (3,8,15,16). Tandem fusion of multiple ADs, including VP64 (V), P65 (P), and Rta (R), to dCas9 (dCas9-VPR) represents the second generation with much higher potency due to synergy among distinct ADs (7). First, we inserted one or two ER^{T2} domains in between dCas9 and VPR (dCas9-E-VPR and dCas9-2E-VPR) or fused ER^{T2}(s) to the C-terminus of the entire construct (dCas9-VPR-E and dCas9-VPR-2E) (Supplementary Figure S1B). We observed robust activation of the luciferase reporter across all four constructs in a gRNA specific manner upon treatment with 4-OHT (Supplementary Figure S1C). In the absence of 4-OHT, no significant background activity was introduced by the dCas9-2ER^{T2}-VPR (dCas9-2E-VPR) construct, in contrast to the other three (Supplementary Figure S1C). In addition, further improvement of activation potency with undetectable background activity was observed when VPR was replaced with VPH (VP64, p65 and HSF1) in the same architecture (dCas9-2E-VPH) (Supplementary Figure S1D). Taken together, HIT-dCas9 activation system based on direct fusion to ER^{T2} domains concluded at dCas9-2E-VPH, which delivered the highest potency upon drug induction without obvious background activity (Figure 1A).

Next we worked on the SAM system, in which minimal MS2 aptamers are appended to the tetraloop and stem loop 2 in the sgRNA scaffold (named sgRNA2.0), which recruit ADs fused to a MS2 binding protein (MCP) (6). The original design involves two hybrid proteins: dCas9-VP64 and MCP-PH. Data showed that AD recruitment to the MS2 sites contributed much more to the potency than that directly fused to dCas9, possibly due to four AD molecules accommodated to the MS2 aptamers (6). Accordingly, we first used a dCas9-NLS construct without VP64 in conjunction with fusion constructs of various ADs to MCP-ER^{T2} (MCP-E) (Supplementary Figure S2A). Additive drug inducible effect was observed upon addition of VP64 to PH or PR (MCP-E-VPH or MCP-E-VPR) (Supplementary Figure S2B). Further addition of another R to VPH (MCP-E-VPHR) rather lowered its potency (Supplementary Figure S2B). Moreover, splitting VPH into VP64 and PH (MCP-E-VP64+PH) displayed similar activation efficiency upon drug induction, indicating intermolecular synergy is not more effective in this arrangement (Supplementary Figure S2B). Taken these data together, we chose VPH as the most efficient AD combination for further optimization. Notably, higher background activity in the absence of 4-OHT accompanied higher potency when using the trimer and tetramer AD constructs (Supplementary Figure S2B). To this end, we fused two ER^{T2} to the MCP-VPH construct (MCP-2E-VPH) and found this significantly lowered the background without compromising the drug induced activity (Supplementary Figure S2C). In addition, further rendering dCas9 to 4-OHT regulation (dcas9-2ER^{T2}, dCas9-2E) appeared not necessary as this dramatically reduced the potency upon drug induction (Supplementary Figure S2C). Therefore, the best design for our optimized HIT-SAM systems concluded at the conjunct use of dCas9-NLS and MCP-2E-VPH, which takes advantage of tight regulation of MCP-VPH *via* fusion with two tandem ER^{T2} domains while increasing the access of dCas9 to its target DNA *via* NLS tagging (Figure 1B).

Another major transactivation system named SUperNova TAGging (SunTag) utilizes specific binding of soluble single chain variable fragment (scFv) antibodies to multiple GCN4 peptides. In this system, VP64 is fused with scFv and recruited to a tandem array of GCN4 peptides fused with dCas9 (10,11). Amplified potency was observed in comparison to the original dCas9-VP64 as multiple VP64 modules were recruited to a single dCas9–gRNA complex. To establish a SunTag based drug inducible transactivation system, we cloned one or two ER^{T2} domains between scFv and ADs (scFv-E-ADs or scFv-2E-ADs), which were then used in conjunction with dCas9-NLS fused with 10 × GCN4 peptides to its C-terminus (dCas9–NLS–GCN4) (Supplementary Figure S3A). Consistent with our previous observations, VPH, VPR and VPHR demonstrated additive domain synergy (Supplementary Figure S3B). As observed in other systems, VPH consistently elicited highest level of activation upon drug induction. Importantly, 2ER^{T2} fusion controlled the background activity in the absence of 4-OHT to a non-significant level in comparison to the negative control across all AD combinations. Furthermore, in contrast to our finding in SAM system, separating VPH into two constructs, V and PH, delivered a more robust synergetic effect, possibly due to higher numbers of AD modules that the SunTag system can accommodate (Supplementary Figure S3C and D). Moreover, similar to the inducible SAM system, replacing NLS tagged dCas9 with one fused with 2ER^{T2} (dCas9-2E-GCN4) significantly reduced the activation potency (Supplementary Figure S3D). Taken together,

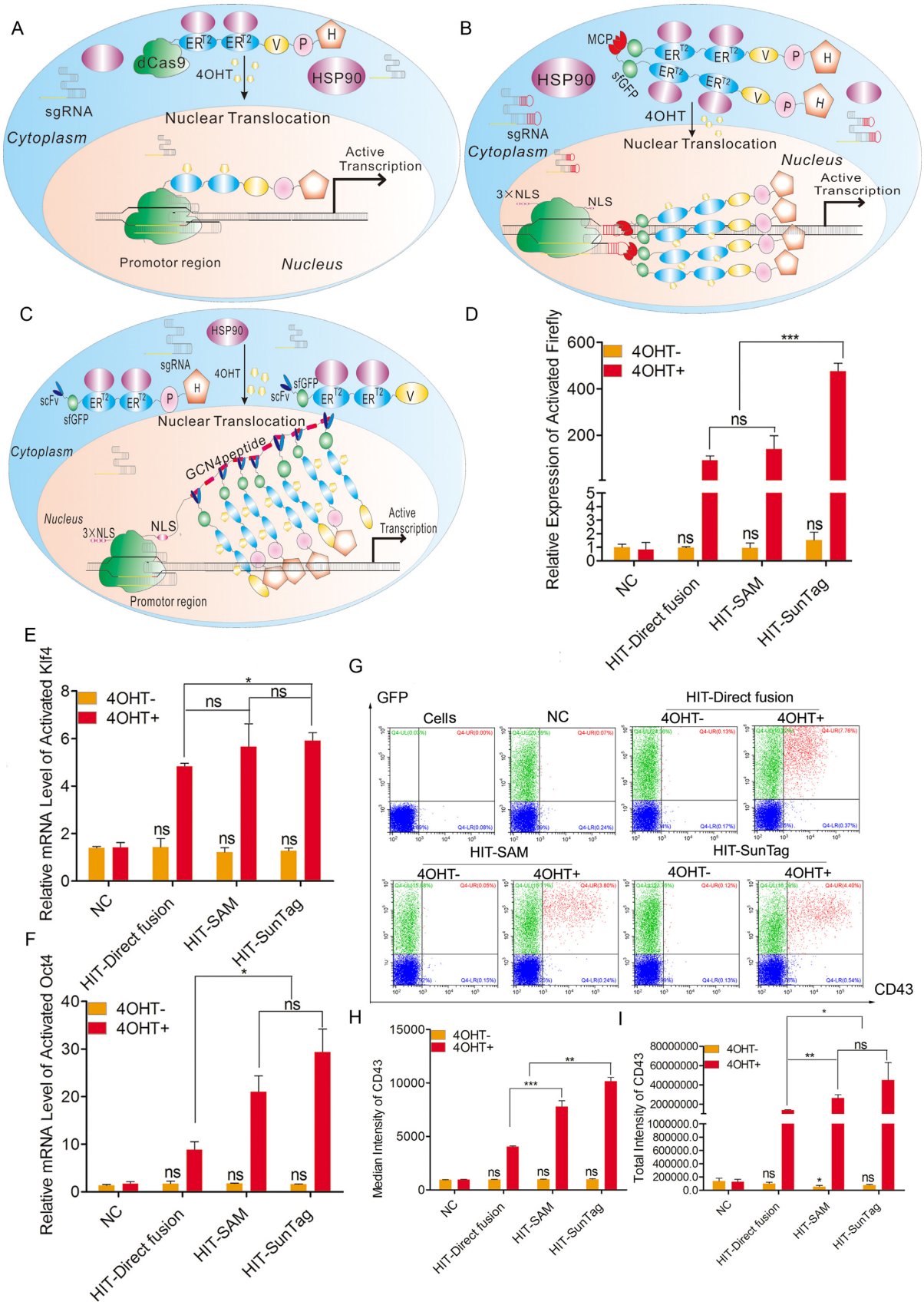

Figure 1. Design, optimization and cross-comparison of HIT transcription activation systems. (**A–C**) Cartoons illuminating the mechanisms of optimized 4-OHT induced transcription activation using a direct fusion HIT construct (A), the HIT-SAM system (B), and the HIT-SunTag system (C). (**D–I**)

we concluded our optimization of HIT-SunTag systems at the co-delivery of dCas9–NLS–GCN4, scFv-2E-VP64 and scFv-2E-PH (Figure 1C).

We have accomplished tight and effective drug induction across all three systems. A pending question is which system delivered the most effective drug inducible performance. To this end, we compared the optimized designs of each system in a carefully controlled manner side-by-side in the same experiment (Figure 1D). We also expanded our analyses to multiple endogenous genes, including Klf4 and Oct4, examined by RT-PCR (Figure 1E and F), and CD43, examined by flow-cytometry (Figure 1G–I). The optimized terminal HIT-SunTag design displayed the highest or the equally highest transcriptional efficiency upon drug treatment across all these assays (Figure 1D–F). Notably, the direct fusion construct dCas9-2E-VPH elicited the lowest level of activation across all assays and its lowest potency could be clearly observed in single cell resolution by flow cytometry, a distinction possibly due to only one VPH module recruited to the promoters (Figure 1D–I). Importantly, background activities in the absence of 4-OHT remained undetectable across all these optimized designs (Figure 1D–I). Next, utilizing these assays cross these endogenous genes, we conducted collateral assessments for selectivity (Supplementary Figure S4). In doing so, we included another cell surface protein CD31 to cross examine it with CD43 for gene activation at the protein level (Supplementary Figure S4A and B). Our results indicate no collateral effect among these sgRNAs in activation of their targets (Supplementary Figure S4), thus implying good specificity in agreement with previous reports examining the original SunTag system (10,12).

HIT2: a drug inducible CRISPR/Cas9 device capable of both transcriptional activation and genome editing

It was reported previously that a shortened sgRNA with less than 16 nucleotides (nt) complementary to its target DNA allows wildtype Cas9 to bind its target without cleaving it (40,41). Taking advantage of this differential effect, we envisioned to use one CRISPR/Cas9 device with sgRNAs in different lengths to simultaneously achieve genome editing and transcriptional activation in a drug inducible manner. Considering the superiority of two tandem ER^{T2} for the control of background activity, we replaced dCas9 with Cas9-$2ER^{T2}$ fusion modules (C2E) in all optimized activation constructs (Supplementary Figure S5A), thus rendering genome editing activity also drug inducible. Using a shortened sgRNA (14 nt), we observed significant 4-OHT induction of luciferase reporter signal and no background activity without the drug (Supplementary Figure S5B). Notably, the activation efficiency of SAM system (C2E + MCP-2E-VPH) was approximately a magnitude lower than direct fusion (C2E-VPH) and SunTag (C2E-GCN4 + scFv-2E-VP64 + scFv-2E-PH), in strong contrast to results using dCas9 and full length sgRNAs (Figure 1D), suggesting that a shortened sgRNA might be less tolerant to MS2 aptamer appendages. We therefore focused on direct fusion and SunTag systems for further interrogations. We also examined genome editing activity of these Cas9-$2ER^{T2}$ (C2E) constructs using a fluorescence conversion reporter (FCR) assay (38), in which BFP is converted to GFP upon HDR mediated substitution of a key amino acid (Supplementary Figure S5C). Surprisingly, GCN4 fusion to C2E in the SunTag system renders higher editing activity upon drug induction in comparison with fusion with VPH and without (Supplementary Figure S5D). And notably, all three constructs introduce significant background activity in the absence of drug treatment (Supplementary Figure S5D). Therefore, in order to attenuate background activity in genome editing, we introduced one or two nuclear export signal (NES) peptides to the C2E-VPH and C2E-GCN4 constructs (Supplementary Figure S6A) (23,42). Drug inducible transcriptional activation was examined using the luciferase reporter assay (Supplementary Figure S6B) and the endogenous CD43 activation assay (Supplementary Figure S6C). A pSSA assay was also employed to examine DNA cleavage activity of these Cas9 constructs, in which a functional luciferase reading frame was restored via single strand annealing (SSA) (Supplementary Figure S7A) (36). Among all tested designs, GCN4 constructs appeared to be highly efficient in both activation with 14nt sgRNAs and editing with 20nt sgRNAs (Supplementary Figures S6 and S7).Our results also validated minimal editing and retained binding activities using wildtype Cas9 and shortened 14nt sgRNAs (40,41). Full length sgRNAs were also capable, but dramatically less efficient, of inducing luciferase signal in a 4-OHT dependent manner, probably due to complication from editing events that impair transcription (Supplementary Figure S6B).

Further focused examinations of Cas9-$2ER^{T2}$-GCN4 (C2E-GCN4) constructs harboring one and two NES peptides respectively (CN2E-GCN4 and C2N2E-GCN4) were conducted across a panel of gene editing assays, including the FCR assay (Supplementary Figure S8), an endogenous CD201 knockout assay (Supplementary Figure S9) and a traffic-light reporter (TLR) assay (37) (Supplementary Figure S10). In the endogenous CD201 knockout assay, we used a sgRNA that effectively targets the 5′ region of the coding sequence of CD201, a cell surface protein highly

←

Cross-comparison among three optimized HIT transcription activation systems. Transcription activation induced by HIT constructs was examined in the luciferase reporter assay (D), by quantification of relative mRNA level of endogenous expression for Klf4 (E) and Oct4 (F), and by flow-cytometry analyses of CD43 protein level on the cell surface (G–I). Representative plots (G) and quantitative analyses of median CD43 fluorescent intensities (H) and overall CD43 fluorescent intensities (I) of CD43+GFP+ positive population were shown. GFP fluorescence indicates successful transfection. Cells transfected with the same amount of reporter construct or sgRNA only while keeping the total amount of transfection constant were used as negative controls (NC) in the luciferase reporter assay. Cells transfected with an ER^{T2} tagged GFP construct while keeping the total amount of transfection constant were used as negative control (NC) in qRT-PCR assays. Cells transfected with an unrelated sgRNA (ctl sgRNA) and GFP were used as negative control (NC) in flow-cytometry analyses. Data showed mean ± SD. $n = 3$ biological replicates. ns: non-significant;*$P < 0.05$; **$P < 0.01$; ***$P < 0.001$; two tailed *t*-tests. Three biological replicates means three independently transfected samples throughout this study. The readouts without drug induction were compared in t-tests against the negative controls (NCs) for background detection.

expressed in human embryonic kidney 293T (HEK 293T) cells, and examined NHEJ induced gene knockout using flow cytometry. The TLR assay can probe both NHEJ and HDR events using a reporter construct in which the restoration of mCherry and GFP signals measure NHEJ and HDR events respectively (Supplementary Figure S10A) (37). Results across all these assays demonstrated a consistent reduction of background activity to minimal level by having two tandem repeats of NES peptides. Therefore, we used C2N2E-GCN4 in conjunction with scFv-2E-VPH, a device we termed 'HIT2', for simultaneous drug inducible genome editing and transcriptional activation (Figure 2A). When co-transfected with a full length sgRNA targeting the BFP coding region and a shortened sgRNA targeting the CD43 promoter, simultaneous editing of BFP to GFP and CD43 activation was accomplished in a drug inducible manner (Figure 2B). When a NLS tagged Cas9–GCN4 construct (Cas9–NLS–GCN4) was used, as expected, editing events were not subject to drug control (Figure 2B).

Upon completion of optimization of HIT and HIT2 systems, we next examined 4-OHT induced subcellular trafficking of the ER^{T2} constructs in the terminal designs. A super folding GFP (sfGFP) is fused with scFv constructs to facilitate protein folding (11), which allows us to examine its subcellular distribution. As expected, both scFv-2E-VP64 and scFv-2E-PH proteins showed drug inducible translocation from the cytoplasm to the nucleus (Supplementary Figure S11). We also cloned a fusion construct of GFP to scFv without any localization signal to objectively probe subcellular localization of the C2N2E-GCN4 construct. scFv-GFP was evenly distributed in cells when transfected alone (Supplementary Figure S12). When co-transfected with C2N2E-GCN4, an obvious cytoplasmic retention was observed. An obvious nuclear accumulation of scFv-GFP was observed upon adding 4-OHT to the culture medium (Supplementary Figure S12). These data support a working mechanism of drug inducible nuclear translocation of our HIT constructs.

Comparison with existing designs

Previously multiple designs of drug inducible CRISPR/Cas9 systems have been reported (21–24). Insertion of an evolved intein within Cas9 at Serine 219 (intein-S219) disrupts its conformation, which is restored upon 4-OHT dependent intein splicing (24). In a split-Cas9 architecture, Cas9 and dCas9 were split into two halves and separately fused with two binding partners of mammalian target of rapamycin (mTOR), FK506 binding protein 12 (FKBP) and FKBP rapamycin binding (FRB) domains. Rapamycin induces binding of the pairs, thus reconstitute Cas9 or dCas9 protein (23). Doxycycline inducible Cas9 systems were also characterized (21,22). We next compared the performance of our HIT-SunTag and HIT2 systems with these published designs head to head in drug inducible transcriptional activation. Since only gene editing intein system was reported in the original paper (24), we cloned its gene construct in which intein (G521R) was inserted into dCas9 at the same site as Cas9. The G521R mutation renders intein refractory to endogenous β-estradiol ligand, a property crucial for selective control by the exogenous 4-OHT (24). VPR, the AD array reported to improve potency (7), was fused to the C-terminus of dCas9. A dCas9-VPR driven by a TRE3G promoter was also constructed. In the luciferase reporter assay, consistent with previous results, we observed no significant background activity and efficient reporter activation using HIT-SunTag system employing dCas9 with a full length sgRNA or HIT2 system (C2N2E-GCN4) with a shortened sgRNA (Figure 3A). In contrast, high background signals for both intein and Tet-on constructs were seen in the absence of chemical induction. The leaky background of the Tet-on system is consistent with its use without doxycycline in independent studies (34,43). All three previously reported designs were significantly less potent than our systems upon drug treatment, partly due to their less optimized AD combinations. Activation of endogenous CD43 expression observed similar differences in drug inducible efficiency between our constructs and published designs (Figure 3B–D). Only Tet-on system showed high background activity in this assay, possibly due to lower sensitivity compared with the one using luciferase reporter. Notably, HIT2, although enabling both activation and editing, did compromise activation potency, possibly due to the use of shortened sgRNAs (Figure 3A–D). Therefore, it is recommended to use HIT-SunTag when simultaneous editing is not desired.

Given that our HIT2 system is armed with extra functionality of drug inducible genome editing, we next benchmarked this activity too. C2N2E-GCN4 used in HIT2 system introduced lower background activity than that from intein-S219-Cas9, Split-Cas9 and TRE3G-Cas9 in the FCR assay (Figure 3E), Consistent with previous observations for activation (Figure 3A–D), TRE3G-Cas9 elicits most pronounced background activity. Intein-S219-G521R-Cas9 displayed non-significant background activity but its drug induced activity is significantly lower than the HIT2. These differences were also observed in the less sensitive TLR assay (Supplementary Figure S13). Taken together, these data demonstrated advantageous performances of our HIT systems for activation and HIT2 for editing over multiple existing designs including intein, split and Tet-on.

Selectivity, titratability, speed and reversibility of drug induction of HIT systems

In addition to the tightness and efficiency, we next further characterized our HIT systems for other important criteria of drug inducible modulation. These include selectivity over endogenous β-estradiol ligand, whether their activities are titratable with different concentrations of 4-OHT, and the speed of drug induced effect and whether it is reversible.

We first examined dose dependent response of optimized terminal HIT-SunTag and HIT2 systems to 4-OHT and β-estradiol respectively. Transcriptional activation was examined in the luciferase reporter assay (Figure 4A and B) and the endogenous CD43 activation assay (Figure 4C and D, Supplementary Figure S14). Selective response to 4-OHT was observed across all these assays for all HIT systems. Dose dependent activities were achieved, a demonstration of titratable response by varying drug concentration. As expected, selective response to 4-OHT over β-estradiol for transcriptional activation was achieved when using intein

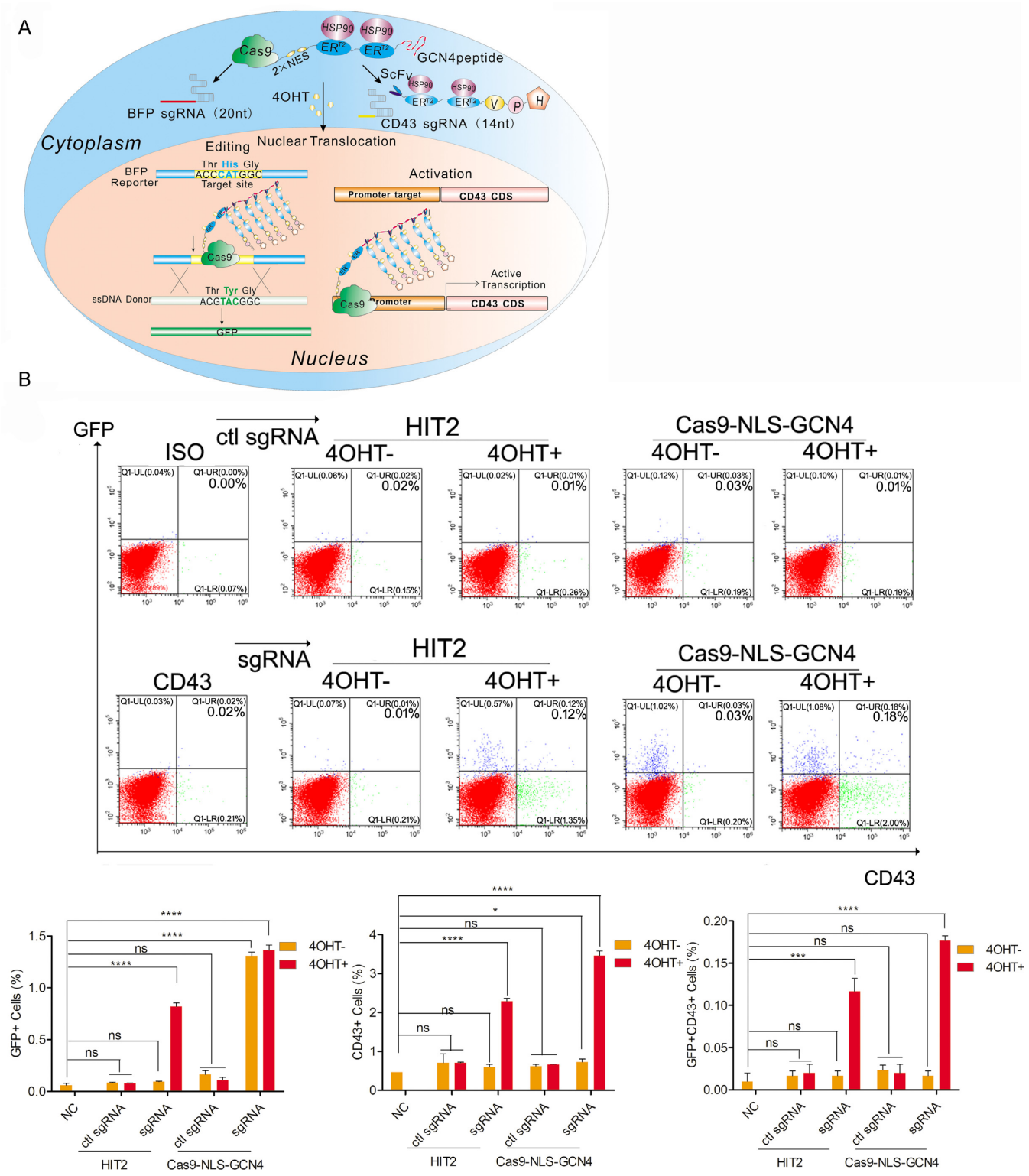

Figure 2. HIT2: one CRISPR/Cas9 device for simultaneous genome editing and transcriptional activation in a drug inducible manner. (**A**) Cartoon illuminating the mechanism of the optimized drug inducible HIT2 system for simultaneous genome editing and transcriptional activation. (**B**) Simultaneous editing and activation by HIT2 and Cas9–NLS–GCN4 were examined using flow-cytometry. The percentage of GFP positive cells indicated HDR efficiency, while CD43 protein level on the cell surface represented transcription activation. Representative plots (upper panels) and quantitative analyses (lower panels) were shown. Data showed mean ± SD. $n = 3$ biological replicates. ns: non-significant;*$P < 0.05$; *** $P < 0.001$; ****$P < 0.0001$; two-tailed t-tests.

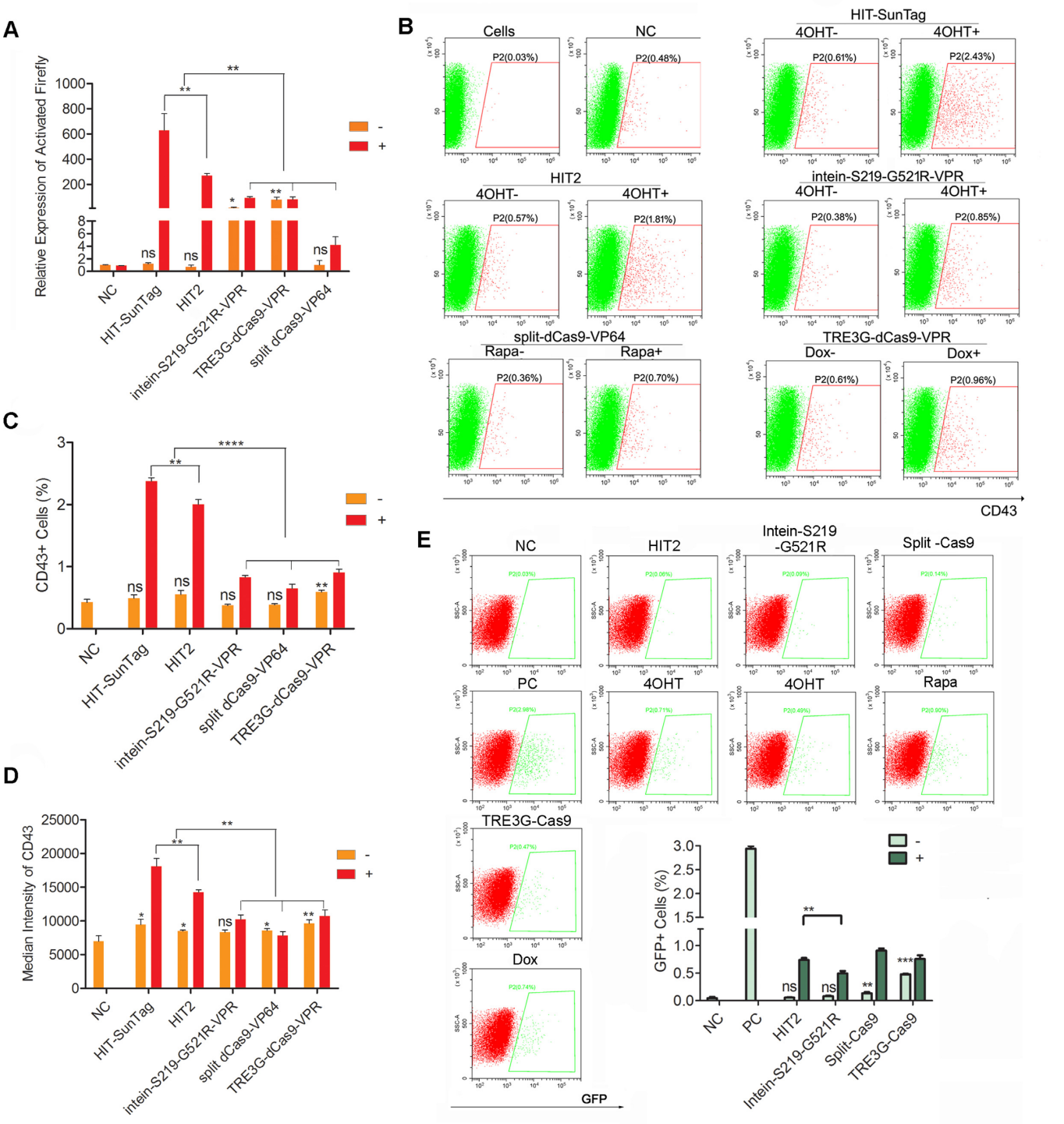

Figure 3. Comparisons of HIT systems with existing drug inducible designs. (**A–D**) Drug inducible efficiency and background activity of transcription activation was examined head-to-head between HIT systems and existing designs using the luciferase reporter assay (A), in which the expression of luciferase was controlled by a sgRNA target sequence (gLuc sgRNA), and the CD43 activation assay (B-D).Representative plots (B), quantitative analyses of the percentage of CD43 positive cells (C), and median CD43 fluorescent intensities (D) were shown. (**E**) Drug inducible efficiency and background activity of genome editing was examined using the FCR assay in comparison with existing designs. Representative plots (top) and quantifications (right bottom) were shown. NC, cells transfected with an unrelated sgRNA; PC, cells transfected with Cas9-NLS and BFP sgRNA. Data showed mean ± SD. $n = 3$ biological replicates. ns: non-significant;*$P < 0.05$; **$P < 0.01$; ****$P < 0.0001$; two-tailed t-tests.

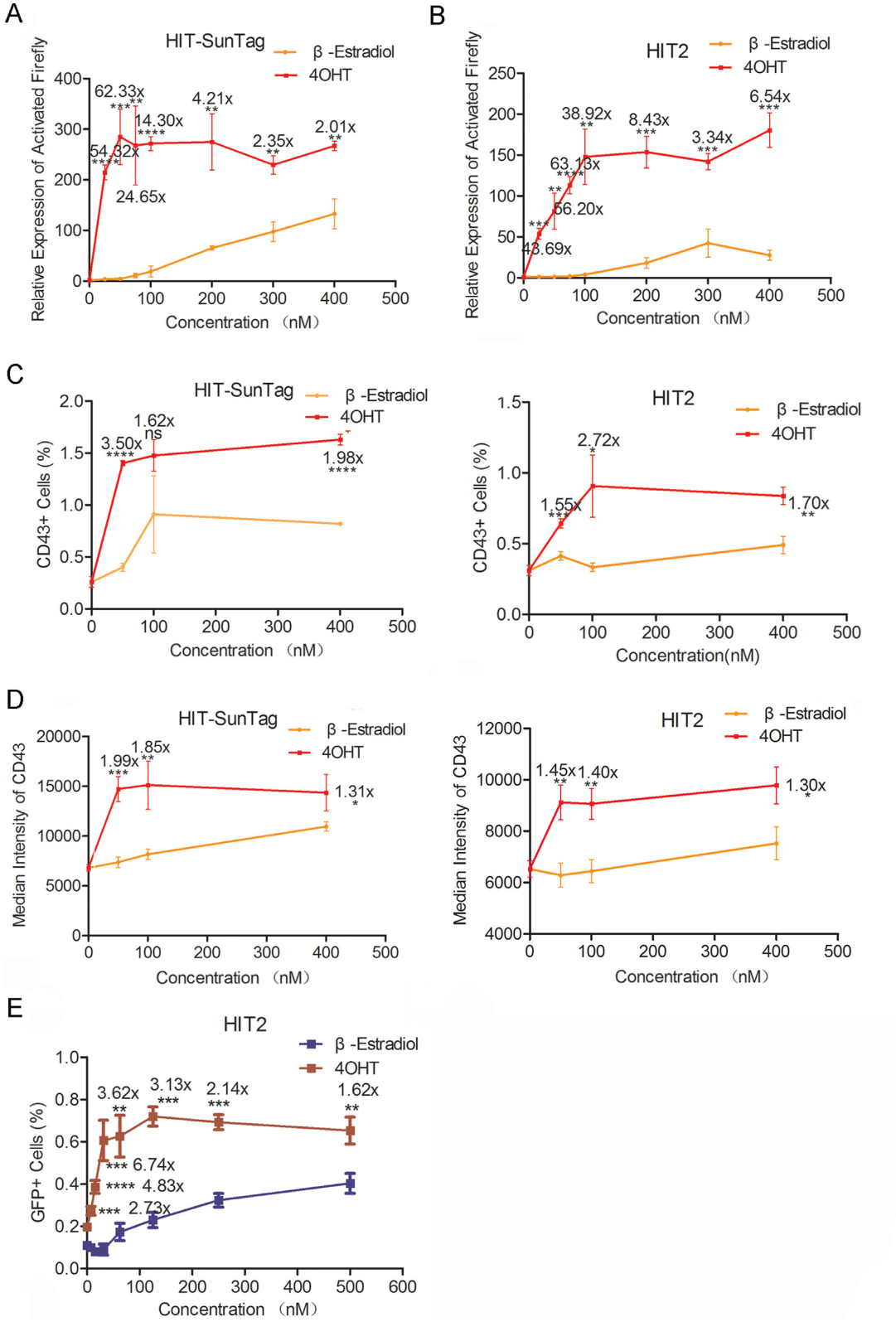

Figure 4. Selective and titratable drug induction of HIT systems. (**A** and **B**) Dose dependent transcription activation induced by HIT-SunTag (A) and HIT2 (B) with different concentration of β-estradiol or 4OHT was examined using the luciferase reporter assay. (**C** and **D**) Activation of endogenous gene CD43 was examined using flow cytometry. Quantitative analyses of the percentage of CD43 positive cells (C) and median CD43 fluorescent intensities (D) were shown. (**E**) Dose dependent genome editing activities of HIT2 were examined using the FCR assay upon treatment with different concentration of β-estradiol or 4-OHT. Data showed mean ± SD. $n = 3$ biological replicates. ns: non-significant; $*P < 0.05$; $**P < 0.01$; $***P < 0.001$; $****P < 0.0001$; two-tailed *t*-tests. Fold of activation by 4-OHT over the same concentration of β-estradiol was displayed.

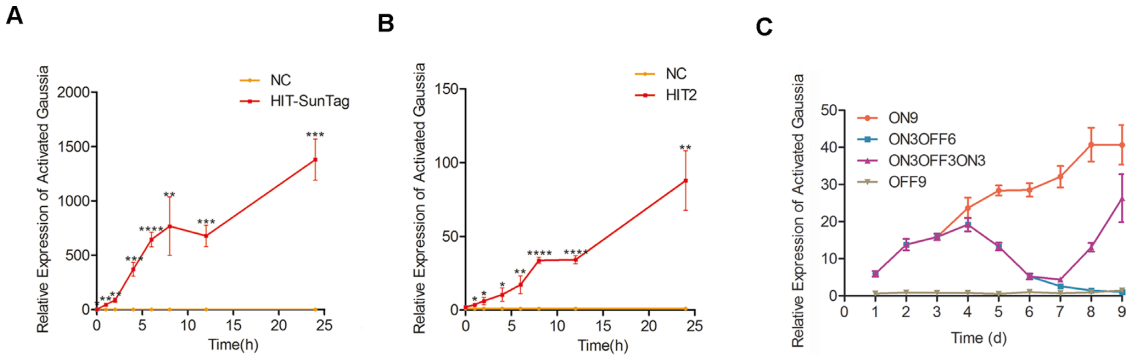

Figure 5. Rapid and reversible drug induction of HIT systems. (**A** and **B**) Luciferase signal was examined upon drug treatment for distinct lengths of time using (A) HIT-SunTag system and (B) HIT2 system. (**C**) Reversibility of HIT-SunTag was examined in a stable cell line expressing the luciferase reporter and HIT-SunTag constructs. Cells were either continuously treated with 250 nM of 4-OHT for 9 days (ON9) or without (OFF9), or treated for 3 days followed by being cultured without 4-OHT for 6 days (ON3OFF6) or treated for 3 days, then cultured without 4-OHT for 3 days followed by the treatment of 4-OHT again for 3 days (ON3 OFF3 ON3), respectively. Data showed mean ± SD. $n = 3$ biological replicates. ns: non-significant;*$P < 0.05$; **$P < 0.01$; ***$P < 0.001$; ****$P < 0.0001$; two-tailed t-tests. The signals activated by HIT systems were compared against the negative controls (NCs).

dCas9 construct that harboring the G521R mutation (Supplementary Figure S15). Nonetheless, our HIT systems displayed higher sensitivity and selectivity than the intein (G521R) construct. A much lower concentration of 4-OHT was required to reach maximum level of activation activity for our HIT constructs than that for the intein (G521R) construct. Fold difference between 4-OHT and β-estradiol was also higher for HIT systems across the dose range of selective response. Consistent with previous results, the maximum activities of HIT systems were also higher than the intein (G521R) construct. In fact, in contrast to HIT systems, selective activity of the intein (G521R) activation construct in response to 4-OHT could not be detected in a less sensitive CD43 activation assay. Examination of editing activity from HIT2 also demonstrated better sensitivity and selectivity than the intein (G521R) system (Figure 4E and Supplementary Figures S16 and S17)

Speed of response and reversibility are essential to achieve precise and dynamic gene regulation using drug inducible transcription modulation systems. Using either HIT-SunTag or HIT2 system, we observed a significant activation as short as 1 h and increase of signal over time in the luciferase assay, an indication of a very rapid response that is also titratable by altering the exposure time (Figure 5A and B). We also examined whether the drug induced effect could be reversed upon drug withdrawal using the HIT-SunTag system. We toggled 4-OHT treatment of a cell line in which HIT-SunTag constructs, the luciferase reporter, and the sgRNA construct targeting its promoter were stably integrated into the genome through lentiviral delivery. A decrease in luciferase signal was observed upon 4-OHT withdrawal and such signal can be reactivated upon re-supply of the drug (Figure 5C). Distinctions in responses could be clearly observed in comparison with continuous treatment, continuous withdrawal, and no treatment groups. Treatments with a different concentration of 4-OHT led to consistent results (Supplementary Figure S18). These results indicate the response of our HIT systems to drug induction is rapid and reversible, which are crucial properties for sensitive and precise control of functional modulation.

Adaptation of HIT designs to orthogonal *Staphylococcus aureus* Cas9

Orthogonal Cas9 species other than the prevalent *Streptococcus pyogenes* (SpCas9), which the current study is based on so far, require distinct PAM sequences, thus expanding the coverage of target loci in the genome (5). They can be used in conjunction to deliver functional perturbations in multiple modes simultaneously. Among them, *Staphylococcus aureus* Cas9 (SaCas9) has attracted much interest because of the high incidence of its PAM sequence (NNGRR), its high activity in mammalian cells, and a smaller size of protein than SpCas9, which is critical to fit certain delivery vehicles for gene therapy with a restrictive cargo size (e.g. adeno-associated virus (AAV)) (30). Therefore, we next explored the feasibility of adapting our optimized HIT designs to the SaCas9 species.

First, we generated a NLS–dSaCas9–GCN4 construct for drug inducible transcriptional activation and use it in conjunction with scFv-2ER^{T2}-AD constructs (Figure 6A). Combination of V and PH constructs introduced a more pronounced activation than V or PH alone. And the drug inducible activation was sgRNA dependent (Figure 6A) and ER^{T2} dependent (Supplementary Figure S19). In an assay to activate endogenous CD43 expression, robust drug inducible action was achieved with minimal background activity (Figure 6B). Conjunct use of such a dSaCas9 HIT-SunTag device with a split dSpCas9-VPH device under control of a different drug, rapamycin, selectively delivered transcriptional activation under their respective drug inductions of both luciferase reporters and endogenous genes (23) (Supplementary Figure S20). Notably, split architecture displayed a much lower efficiency upon drug induction even AD was changed from V to the more potent VPH combination, which was difficult to detect in the less sensitive endogenous gene activation assay. Next, to deliver both editing and activation using a HIT2 device, we first explored whether sgRNA length variation plays a similar role in control of binding and editing as that for SpCas9. We cotransfected wildtype SaCas9 with sgRNAs in varying lengths and examined them in both the pSSA assay for editing activity (Supplementary Figure S21A) and the luciferase acti-

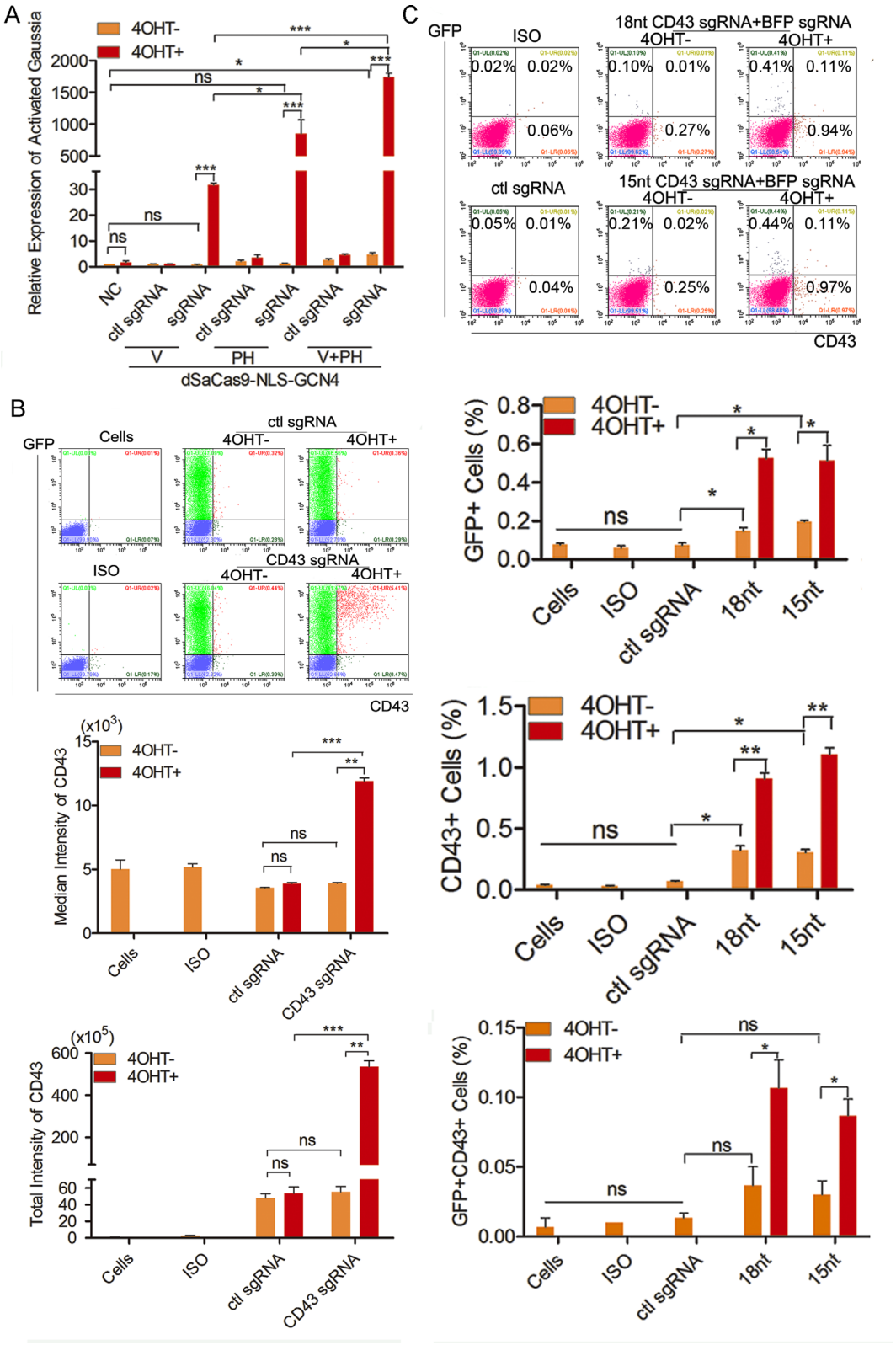

Figure 6. Adaptation of HIT designs to SaCas9. (**A** and **B**) Drug inducible gene activation by NLS-dSaCas9–GCN4 in conjunction with scFv-2ER^{T2}-AD was examined in the luciferase reporter assay (A) and the endogenous CD43 activation assay (B). (**C**) Simultaneous genome editing and transcriptional activation by HIT2-SaCas9 were examined by the FCR activity and CD43 activation respectively. Cells transfected with the same amount of reporter construct while keeping the total amount of transfection constant were used as negative controls (NC). ISO represents cells stained with antibody isotype control. Data showed mean ± SD. $n = 3$ biological replicates. ns: non-significant;*$P < 0.05$; **$P < 0.01$; ***$P < 0.001$; two-tailed t-tests.

vation assay (Supplementary Figure S21B). Shortening the sgRNA target complementary sequence by 1nt almost completely abolishes its editing activity while a target complementary sequences at 15nt to 18nt is most efficient in activation. Accordingly, we constructed SaCas9-2NES-2ER^{T2}-GCN4 and co-transfected it with a full length sgRNA for BFP editing and a sgRNA either at a length of 15nt or 18nt to activate CD43. As a result, simultaneous editing and activation in a drug inducible manner was delivered using HIT2-SaCas9 constructs with shortened sgRNAs in either length (Figure 6C). Taken together, using SaCas9 as an example, we demonstrated that our HIT designs may be adapted to orthogonal species, thus further expanding their uses.

DISCUSSION

In summary, upon vigorous optimization of a number of designs, we have established multiple advantageous drug inducible devices for transcription activation by coupling ER^{T2} with various CRISPR/Cas9 systems, and further empowered the most effective system with extra editing functionality. Differences in distinct systems can be difficult to uncover due to confounding variables, such as different batch of cells, different transfection efficiencies. To eliminate these complications as much as we could, we always examined different designs side by side in the same experiment and conducted multiple assays to make definitive comparisons. We also carefully conducted these experiments in a well-controlled manner such as matching the molar amount of constructs that contain dCas9 or Cas9, sgRNAs and ADs respectively across different designs. Tight and efficient drug induction of transcription activation was achieved by conjunct delivery of NLS-dCas9–GCN4, scFv-2E-VP64 and scFv-2E-PH, a HIT-SunTag system with improved potency (Figure 1D-I; Supplementary Figure S3). Further, utilizing differential activities of DNA cutting and binding with sgRNAs in varying lengths, simultaneous editing and activation was accomplished with one device we named HIT2 that consists of C2N2E-GCN4, scFv-2E-VPH (Figure 2). Cross-comparisons with other designs demonstrated better performances of the HIT systems (Figures 3 and 4; Supplementary Figures S13–S17). We did not focus on the split design because of its interference against mTOR, a central pathway in many biological processes (44). Nonetheless, a latest report deployed ER^{T2} domain on top of this design to reduce its background activity, consistent with our observations of ER^{T2} as tight regulator of drug induction (26). The current study focused on transcription activation and further harnessed the power of our optimized system by enabling simultaneous editing in a drug inducible manner. Two recent reports, which described drug inducible editing devices by fusion of four ER^{T2} domains to Cas9 and by insertion of a ER ^{T2} domain into Cas9, lend more support to the utility of ER^{T2} as a tight and effective tool for drug inducible control (25,27). Last but not the least, successful adoption of HIT designs to SaCas9 in the current study suggests further expansion of their applications (Figure 6).

Better understanding of the ER^{T2} based drug induction and various designs of Cas9 systems from this study would also benefit future development of similar molecular devices. First, tandem fusion of 2-ER^{T2}may confer tighter control of drug induction (Supplementary Figures S1-S3) and NES may be employed to reduce background level of ER^{T2}constructs possibly due to reduced nuclear retention of hybrid proteins (Supplementary Figures S8–S10). Second, HIT constructs are responsive to the endogenous ER ligand β-estradiol, albeit at a much lower level than the synthetic 4-OHT (Figure 4 and Supplementary Figures S14 and S16). This suggests opportunities for further improvement on selectivity, which might be accomplished by development of new ER variants as the current one was developed two decades ago (18). Moreover, in the HIT-SAM and HIT-SunTag systems, tandem ER^{T2} fusions to scFv or MCP hybrid proteins were sufficient for a tight control while maximizing dCas9's access to its genomic target DNA enhances its efficiency (Supplementary Figures S2C and S3D). Moreover, VPH combination showed the highest efficiency across multiple scenarios (Supplementary Figures S1D, S2B and S3B) and splitting VPH to V+PH exhibited higher synergy in the HIT-SunTag system (Supplementary Figure S3C and S3D). The HIT designs can be potentially applied to develop next generation CRISPR/Cas9 systems for additional functional perturbations such as transcriptional repression and epigenetic modulation (4,5). Further, the current study used the SaCas9 to demonstrate the applicability of our designs to orthogonal species. Future development of additional systems using engineered SpCas9 with distinct PAM requirements (45), or programmable nucleases from other species (5), will further expand the repertoire of genomic loci and the complexity for functional perturbations. In doing so, HIT-SunTag architecture might be more straightforward as only protein engineering of 'dead' programmable nucleases is needed while shortening gRNA for ramification of binding and editing capabilities might impose extra challenges for HIT2 adaption. Fortunately, preliminary tests paved the way for such adaption to SaCas9 in the current study (Supplementary Figure S21), which will need to be conducted when working on new species in the future.

SUPPLEMENTARY DATA

Supplementary Data are available at NAR Online.

ACKNOWLEDGEMENTS

We thank Dr Andrew P. McMahon (University of South California, CA, USA), Dr Christopher T. Walsh (Harvard Medical School, MA, USA) and Dr Qi Zhou (Institute of Zoology, Chinese Academy of Sciences, Beijing, China) for discussion and reading of this manuscript. We are grateful for all the members of the Wang lab for helpful discussions and technical assistance.

Authors Contributions: Y.W. conceived and supervised the study. J.L., C.Z., Y.Z., J.Z., Y.Z., L.C., Q.H., Y.Y., S.P., R.A. and Y.W. designed experiments. J.L., C.Z., Y.Z., J.Z., Y.Z., L.C., Q.H., Y.Y., S.P. and R.A. performed experiments. J.L., C.Z., Y.Z., J.Z., Y.Z., L.C., Q.H., Y.Y., S.P., R.A. and Y.W. analyzed data. J.L., C.Z., Y.Z., J.Z., Y.Z., L.C. and Y.W. wrote the manuscript.

FUNDING

National Basic Research Program of China [2015CB964800, 2014CB964900]; National Natural Science Foundation of China [31571514, 21402195, 31401270]; Hundred Talents Program of Chinese Academy of Sciences; State Key Laboratory of Stem Cell and Reproductive Biology. Funding for open access charge: State Key Laboratory of Stem Cell and Reproductive Biology.

Conflict of interest statement. Patents covering the novel designs in this work have been filed.

REFERENCES

1. Cong,L., Ran,F.A., Cox,D., Lin,S., Barretto,R., Habib,N., Hsu,P.D., Wu,X., Jiang,W., Marraffini,L.A. *et al.* (2013) Multiplex genome engineering using CRISPR/Cas systems. *Science*, **339**, 819–823.
2. Jinek,M., Chylinski,K., Fonfara,I., Hauer,M., Doudna,J.A. and Charpentier,E. (2012) A programmable dual-RNA-guided DNA endonuclease in adaptive bacterial immunity. *Science*, **337**, 816–821.
3. Mali,P., Yang,L., Esvelt,K.M., Aach,J., Guell,M., Dicarlo,J.E., Norville,J.E. and Church,G.M. (2013) RNA-guided human genome engineering via Cas9. *Science*, **339**, 823–826.
4. Dominguez,A.A., Lim,W.A. and Qi,L.S. (2016) Beyond editing: repurposing CRISPR-Cas9 for precision genome regulation and interrogation. *Nat. Rev. Mol. Cell Biol.*, **17**, 5–15.
5. Mali,P., Esvelt,K.M. and Church,G.M. (2013) Cas9 as a versatile tool for engineering biology. *Nat. Methods*, **10**, 957–963.
6. Konermann,S., Brigham,M.D., Trevino,A.E., Joung,J., Abudayyeh,O.O., Barcena,C., Hsu,P.D., Habib,N., Gootenberg,J.S., Nishimasu,H. *et al.* (2015) Genome-scale transcriptional activation by an engineered CRISPR-Cas9 complex. *Nature*, **517**, 583–588.
7. Chavez,A., Scheiman,J., Vora,S., Pruitt,B.W., Tuttle,M., E,P.R.I., Lin,S., Kiani,S., Guzman,C.D., Wiegand,D.J. *et al.* (2015) Highly efficient Cas9-mediated transcriptional programming. *Nat Methods*, **12**, 326–328.
8. Perez-Pinera,P., Kocak,D.D., Vockley,C.M., Adler,A.F., Kabadi,A.M., Polstein,L.R., Thakore,P.I., Glass,K.A., Ousterout,D.G., Leong,K.W. *et al.* (2013) RNA-guided gene activation by CRISPR-Cas9-based transcription factors. *Nat. Methods*, **10**, 973–976.
9. Chakraborty,S., Ji,H., Kabadi,A.M., Gersbach,C.A., Christoforou,N. and Leong,K.W. (2014) A CRISPR/Cas9-based system for reprogramming cell lineage specification. *Stem Cell Rep.*, **3**, 940–947.
10. Gilbert,L.A., Horlbeck,M.A., Adamson,B., Villalta,J.E., Chen,Y., Whitehead,E.H., Guimaraes,C., Panning,B., Ploegh,H.L., Bassik,M.C. *et al.* (2014) Genome-scale CRISPR-mediated control of gene repression and activation. *Cell*, **159**, 647–661.
11. Tanenbaum,M.E., Gilbert,L.A., Qi,L.S., Weissman,J.S. and Vale,R.D. (2014) A protein-tagging system for signal amplification in gene expression and fluorescence imaging. *Cell*, **159**, 635–646.
12. Chavez,A., Tuttle,M., Pruitt,B.W., Ewen-Campen,B., Chari,R., Ter-Ovanesyan,D., Haque,S.J., Cecchi,R.J., Kowal,E.J., Buchthal,J. *et al.* (2016) Comparison of Cas9 activators in multiple species. *Nat. Methods*, **13**, 563–567.
13. Cheng,A.W., Jillette,N., Lee,P., Plaskon,D., Fujiwara,Y., Wang,W., Taghbalout,A. and Wang,H. (2016) Casilio: a versatile CRISPR-Cas9-Pumilio hybrid for gene regulation and genomic labeling. *Cell Res.*, **26**, 254–257.
14. Cheng,A.W., Wang,H., Yang,H., Shi,L., Katz,Y., Theunissen,T.W., Rangarajan,S., Shivalila,C.S., Dadon,D.B. and Jaenisch,R. (2013) Multiplexed activation of endogenous genes by CRISPR-on, an RNA-guided transcriptional activator system. *Cell Res.*, **23**, 1163–1171.
15. Gilbert,L.A., Larson,M.H., Morsut,L., Liu,Z., Brar,G.A., Torres,S.E., Stern-Ginossar,N., Brandman,O., Whitehead,E.H., Doudna,J.A. *et al.* (2013) CRISPR-mediated modular RNA-guided regulation of transcription in eukaryotes. *Cell*, **154**, 442–451.
16. Maeder,M.L., Linder,S.J., Cascio,V.M., Fu,Y., Ho,Q.H. and Joung,J.K. (2013) CRISPR RNA-guided activation of endogenous human genes. *Nat. Methods*, **10**, 977–979.
17. Metzger,D., Clifford,J., Chiba,H. and Chambon,P. (1995) Conditional site-specific recombination in mammalian cells using a ligand-dependent chimeric Cre recombinase. *Proc. Natl. Acad. Sci. U.S.A.*, **92**, 6991–6995.
18. Feil,R., Wagner,J., Metzger,D. and Chambon,P. (1997) Regulation of Cre recombinase activity by mutated estrogen receptor ligand-binding domains. *Biochem. Biophys. Res. Commun.*, **237**, 752–757.
19. Indra,A.K., Warot,X., Brocard,J., Bornert,J.M., Xiao,J.H., Chambon,P. and Metzger,D. (1999) Temporally-controlled site-specific mutagenesis in the basal layer of the epidermis: comparison of the recombinase activity of the tamoxifen-inducible Cre-ER(T) and Cre-ER(T2) recombinases. *Nucleic Acids Res.*, **27**, 4324–4327.
20. Branda,C.S. and Dymecki,S.M. (2004) Talking about a revolution: The impact of site-specific recombinases on genetic analyses in mice. *Dev. Cell*, **6**, 7–28.
21. Gonzalez,F., Zhu,Z., Shi,Z.D., Lelli,K., Verma,N., Li,Q.V. and Huangfu,D. (2014) An iCRISPR platform for rapid, multiplexable, and inducible genome editing in human pluripotent stem cells. *Cell Stem Cell*, **15**, 215–226.
22. Dow,L.E., Fisher,J., O'Rourke,K.P., Muley,A., Kastenhuber,E.R., Livshits,G., Tschaharganeh,D.F., Socci,N.D. and Lowe,S.W. (2015) Inducible in vivo genome editing with CRISPR-Cas9. *Nat. Biotechnol.*, **33**, 390–394.
23. Zetsche,B., Volz,S.E. and Zhang,F. (2015) A split-Cas9 architecture for inducible genome editing and transcription modulation. *Nat. Biotechnol.*, **33**, 139–142.
24. Davis,K.M., Pattanayak,V., Thompson,D.B., Zuris,J.A. and Liu,D.R. (2015) Small molecule-triggered Cas9 protein with improved genome-editing specificity. *Nat. Chem. Biol.*, **11**, 316–318.
25. Liu,K.I., Ramli,M.N., Woo,C.W., Wang,Y., Zhao,T., Zhang,X., Yim,G.R., Chong,B.Y., Gowher,A., Chua,M.Z. *et al.* (2016) A chemical-inducible CRISPR-Cas9 system for rapid control of genome editing. *Nat. Chem. Biol.*, **12**, 980–987.
26. Nguyen,D.P., Miyaoka,Y., Gilbert,L.A., Mayerl,S.J., Lee,B.H., Weissman,J.S., Conklin,B.R. and Wells,J.A. (2016) Ligand-binding domains of nuclear receptors facilitate tight control of split CRISPR activity. *Nat. Commun.*, **7**, 12009.
27. Oakes,B.L., Nadler,D.C., Flamholz,A., Fellmann,C., Staahl,B.T., Doudna,J.A. and Savage,D.F. (2016) Profiling of engineering hotspots identifies an allosteric CRISPR-Cas9 switch. *Nat. Biotechnol.*, **34**, 646–651.
28. Zhang,F., Cong,L., Lodato,S., Kosuri,S., Church,G.M. and Arlotta,P. (2011) Efficient construction of sequence-specific TAL effectors for modulating mammalian transcription. *Nat. Biotechnol.*, **29**, 149–153.
29. Ding,Y., Ai,H.W., Hoi,H. and Campbell,R.E. (2011) Forster resonance energy transfer-based biosensors for multiparameter ratiometric imaging of Ca2+ dynamics and caspase-3 activity in single cells. *Anal. Chem.*, **83**, 9687–9693.
30. Ran,F.A., Cong,L., Yan,W.X., Scott,D.A., Gootenberg,J.S., Kriz,A.J., Zetsche,B., Shalem,O., Wu,X., Makarova,K.S. *et al.* (2015) In vivo genome editing using Staphylococcus aureus Cas9. *Nature*, **520**, 186–191.
31. Doench,J.G., Fusi,N., Sullender,M., Hegde,M., Vaimberg,E.W., Donovan,K.F., Smith,I., Tothova,Z., Wilen,C., Orchard,R. *et al.* (2016) Optimized sgRNA design to maximize activity and minimize off-target effects of CRISPR-Cas9. *Nat. Biotechnol.*, **34**, 184–191.
32. Doench,J.G., Hartenian,E., Graham,D.B., Tothova,Z., Hegde,M., Smith,I., Sullender,M., Ebert,B.L., Xavier,R.J. and Root,D.E. (2014) Rational design of highly active sgRNAs for CRISPR-Cas9-mediated gene inactivation. *Nat. Biotechnol.*, **32**, 1262–1267.
33. Hsu,P.D., Scott,D.A., Weinstein,J.A., Ran,F.A., Konermann,S., Agarwala,V., Li,Y., Fine,E.J., Wu,X., Shalem,O. *et al.* (2013) DNA targeting specificity of RNA-guided Cas9 nucleases. *Nat. Biotechnol.*, **31**, 827–832.
34. Chen,B., Gilbert,L.A., Cimini,B.A., Schnitzbauer,J., Zhang,W., Li,G.W., Park,J., Blackburn,E.H., Weissman,J.S., Qi,L.S. *et al.* (2013) Dynamic imaging of genomic loci in living human cells by an optimized CRISPR/Cas system. *Cell*, **155**, 1479–1491.
35. Chen,B., Hu,J., Almeida,R., Liu,H., Balakrishnan,S., Covill-Cooke,C., Lim,W.A. and Huang,B. (2016) Expanding the CRISPR imaging toolset with Staphylococcus aureus Cas9 for simultaneous imaging of multiple genomic loci. *Nucleic Acids Res.*, **44**, e75.

36. Bhakta,M.S. and Segal,D.J. (2010) The generation of zinc finger proteins by modular assembly. *Methods Mol. Biol.*, **649**, 3–30.
37. Certo,M.T., Ryu,B.Y., Annis,J.E., Garibov,M., Jarjour,J., Rawlings,D.J. and Scharenberg,A.M. (2011) Tracking genome engineering outcome at individual DNA breakpoints. *Nat. Methods*, **8**, 671–676.
38. Richardson,C.D., Ray,G.J., DeWitt,M.A., Curie,G.L. and Corn,J.E. (2016) Enhancing homology-directed genome editing by catalytically active and inactive CRISPR-Cas9 using asymmetric donor DNA. *Nat. Biotechnol.*, **34**, 339–344.
39. Shechner,D.M., Hacisuleyman,E., Younger,S.T. and Rinn,J.L. (2015) Multiplexable, locus-specific targeting of long RNAs with CRISPR-Display. *Nat. Methods*, **12**, 664–670.
40. Kiani,S., Chavez,A., Tuttle,M., Hall,R.N., Chari,R., Ter-Ovanesyan,D., Qian,J., Pruitt,B.W., Beal,J., Vora,S. *et al.* (2015) Cas9 gRNA engineering for genome editing, activation and repression. *Nat. Methods*, **12**, 1051–1054.
41. Dahlman,J.E., Abudayyeh,O.O., Joung,J., Gootenberg,J.S., Zhang,F. and Konermann,S. (2015) Orthogonal gene knockout and activation with a catalytically active Cas9 nuclease. *Nat. Biotechnol.*, **33**, 1159–1161.
42. Ortiz,O., Wurst,W. and Kuhn,R. (2013) Reversible and tissue-specific activation of MAP kinase signaling by tamoxifen in Braf(V637)ER(T2) mice. *Genesis*, **51**, 448–455.
43. Knight,S.C., Xie,L., Deng,W., Guglielmi,B., Witkowsky,L.B., Bosanac,L., Zhang,E.T., El Beheiry,M., Masson,J.B., Dahan,M. *et al.* (2015) Dynamics of CRISPR-Cas9 genome interrogation in living cells. *Science*, **350**, 823–826.
44. Shimobayashi,M. and Hall,M.N. (2014) Making new contacts: the mTOR network in metabolism and signalling crosstalk. *Nat. Rev. Mol. Cell Biol.*, **15**, 155–162.
45. Kleinstiver,B.P., Prew,M.S., Tsai,S.Q., Topkar,V.V., Nguyen,N.T., Zheng,Z., Gonzales,A.P., Li,Z., Peterson,R.T., Yeh,J.J. *et al.* (2015) Engineered CRISPR-Cas9 nucleases with altered PAM specificities. *Nature*, **523**, 481–485.